

Novel Sulfonated Block Copolymer Containing Pendant Alkylsulfonic Acids: Syntheses, Unique Morphologies, and Applications in Proton Exchange Membrane

HSING-CHIEH LEE, HERMAN LIM, WEI-FANG SU, CHI-YANG CHAO

Department of Materials Science and Engineering, National Taiwan University, Taipei 106, Taiwan

Received 15 January 2011; accepted 26 February 2011

DOI: 10.1002/pola.24655

Published online 8 April 2011 in Wiley Online Library (wileyonlinelibrary.com).

ABSTRACT: In this article, we report the syntheses and characterizations of a series of novel block polyelectrolytes, poly(styrene-*block*-sulfonated hydroxystyrene) (PS-*b*-sPHS), containing pendant sulfonic acid groups attached to the backbone via propyl spacers in the sPHS domain. PS-*b*-sPHS with various compositions were synthesized via anionic polymerization and the following analogous chemistry to achieve accurate control of molecular weight (M_w), narrow polydispersity and high degree of sulfonation. Proton exchange membranes (PEMs) were prepared from PS-*b*-sPHS with sulfonic acids in either potassium salts or tetra-alkylammonium salts via solvent casting and following treatments. Some unique morphologies, such as hollow channels and lamellar arrangement of strings of beads, were observed as a consequence of equilibrium between

microphase separation and columbic interactions between polyelectrolytes. The transportation properties were found to closely relate to the morphologies of the PEMs. The combination of microphase separation of block polyelectrolytes and freedom of movement of pendant alkylsulfonic acids was demonstrated to effectively enhance the proton transport and suppress the methanol crossover for the PEMs, leading to the selectivity higher than Nafion 117 by five times at most. © 2011 Wiley Periodicals, Inc. *J Polym Sci Part A: Polym Chem* 49: 2325–2338, 2011

KEYWORDS: anionic polymerization; block copolymer; block polyelectrolyte; DMFC; methanol crossover; proton exchange membranes; self-assembly

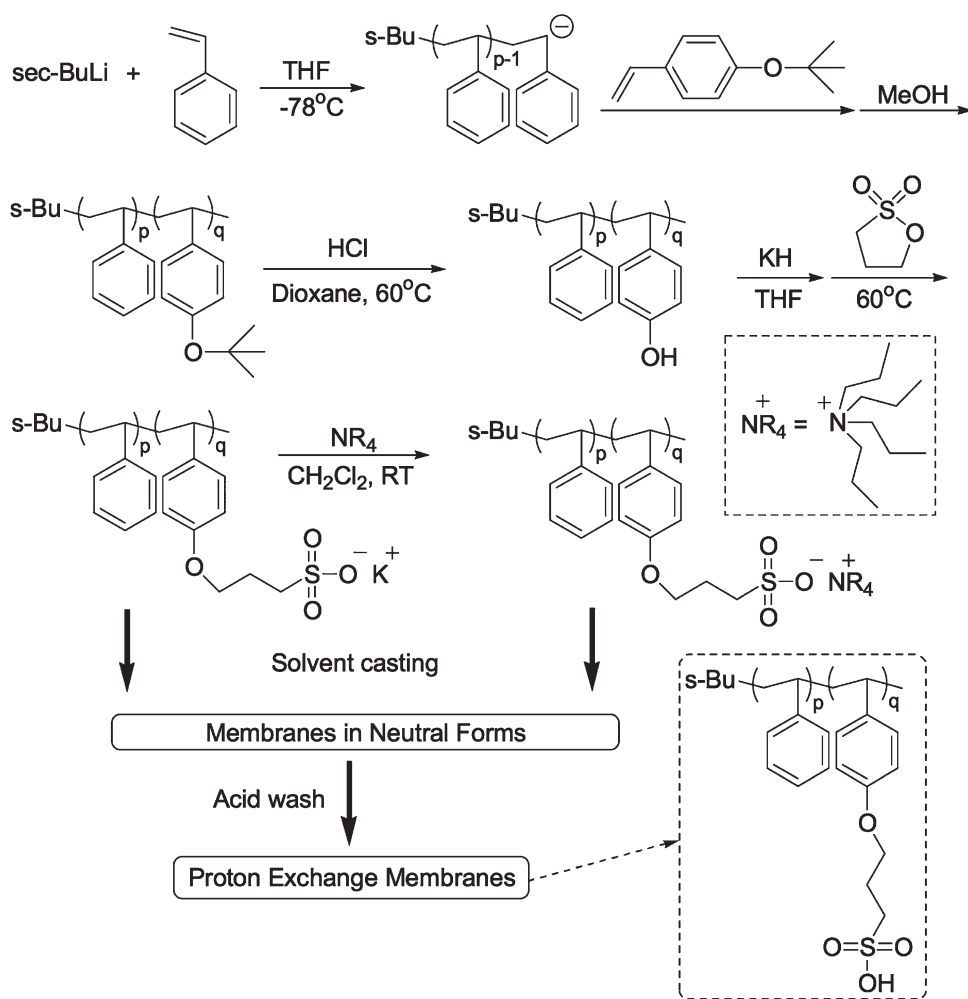
INTRODUCTION Direct methanol fuel cells (DMFCs) have drawn tremendous attention as alternative power sources due to their high efficiencies, environmental benignity, and the use of portable and inexpensive fuel.^{1,2} So far, the critical factors preventing DMFCs from successful commercialization are mainly associated with slow reaction kinetics at anode and methanol crossover from anode to cathode through the proton exchange membrane (PEM), a solid electrolyte to separate the electrodes and to conduct proton from anode to cathode.^{3–5} Methanol crossover would lead to a decrease in open circuit voltage resulting in a suppression of overall cell efficiency, a decline in the fuel utilization efficiency, as well as a shortening of the lifetime.^{6–8} Thus, a successful PEM for DMFC should exhibit high proton conductivity, low methanol permeability, good thermal and dimensional stability, good mechanical strength as well as long-term electrochemical durability.⁹

Nafion®, the mostly used polyelectrolyte for PEM in DMFC, is consisted of a hydrophobic fluorocarbon backbone and perfluoroether side chains with sulfonic acids at the chain ends and it exhibited microphase separated structures with continuous hydrophilic clusters for efficient proton transportation.^{10,11} Although Nafion® membranes exhibit high proton

conductivities and good thermal, chemical, and oxidative stability, the high methanol permeability severely limits the performance of the corresponding DMFC since the channels for proton transportation are also good pathways for methanol permeation. In addition, the strong affinity between methanol and fluorocarbons might considerably worsen the methanol crossover.¹²

Block copolymers with narrow molecular weight distribution are capable of facilitating well-ordered self-assembled nanostructure driven by microphase separation as a result of thermodynamic incompatibility between different blocks.^{13–15} Block polyelectrolytes¹⁶ composed of a hydrophobic segment and a hydrophilic segment containing sulfonic acids were employed for the PEMs owing to their microphase separated morphologies, enabling the formation of continuous proton transportation domain. Furthermore, the transport properties of the PEMs can be tailored by altering the compositions, the degree of sulfonation¹⁷ and the molecular weights of the building blocks. Sulfonated poly(styrene-*block*-ethylene-*random*-butylene-*b*-styrene) (s-SEBS), obtained from postsulfonation of the polystyrene segment of SEBS, were the most studied block polyelectrolyte. The proton conductivity and the methanol permeability of the membrane prepared from

Additional Supporting Information may be found in the online version of this article. Correspondence to: C.-Y. Chao (E-mail: cychao138@ntu.edu.tw)
Journal of Polymer Science Part A: Polymer Chemistry, Vol. 49, 2325–2338 (2011) © 2011 Wiley Periodicals, Inc.



s-SEBS with 37 mol % degree of sulfonation (IEC was similar to that of Nafion 117) simultaneously decreased to half of those values for Nafion 117, suggesting the similarity between the selectivity of *s*-SEBS and of Nafion 117.^{18–20} Kim and coworkers also investigated the solvent effect on the morphologies and the transport properties of *s*-SEBS membranes.^{20–22} Sulfonated poly(styrene-*block*-isobutylene-*block*-styrene) (*s*-SIBS), an analogue of *s*-SEBS, revealed similarities to the *s*-SEBS membranes in proton conductivity, methanol permeability, selectivity and solvent effect.^{23–26} Other block polyelectrolytes studied include sulfonated polystyrene-*block*-poly(dimethylsiloxane) (*s*PS-*b*-PDMS),²⁷ sulfonated poly(styrene-*block*-ethylene) (*s*-SE),²⁸ sulfonated hydrogenated poly(styrene-*block*-butadiene) rubber (*s*-HSBR),²⁹ sulfonated polystyrene-*block*-poly(methyl methacrylate) (*s*PS-*b*-PMMA),³⁰ polystyrenesulfonate-*block*-polymethylbutylene (PSS-*b*-PMB)^{31–33} and sulfonated polybenzimidazoles.^{34,35} In general, the transport properties of the PEMs prepared from the hydrocarbon ionic block copolymers were found to closely relate to their morphologies. In comparison with Nafion® 117 having similar IEC, most of these PEMs showed simultaneous decrements in methanol crossover and proton conductivity, leading to similarity in selectivity.^{18,23,26,27,29} Moreover, the much higher water uptake and

methanol uptake of these membranes might be an issue for dimensional stability.

To achieve high proton conductivity and low methanol crossover simultaneously, our molecular design strategy was to incorporate flexible alkyl spacers between the sulfonic acids and the polymer backbone, instead of the direct attachment of $-\text{SO}_3\text{H}$ to the polymer backbone in most aforementioned polymers, to provide the $-\text{SO}_3\text{H}$ more freedom in movement and thus enhance the relay motion of proton to improve the proton conductivity. The use of alkyl spacers have been demonstrated to be a successful approach in some systems based on poly(aryl ether).^{36,37} Moreover, the spacers might occupy some spaces in the proton transport channels to provide blockage for methanol crossover.

In this work, we synthesized a series of novel block polyelectrolytes, poly(styrene-*block*-sulfonated hydroxystyrene) (PS-*b*-sPHS), comprising of a hydrophobic polystyrene segment and one or two hydrophilic sulfonated polyhydroxystyrene (sPHS) segment(s) containing pendant sulfonic acids attached to the backbone via alkyl spacers (Scheme 1). Anionic polymerization was employed to synthesize the precursor block copolymers poly(styrene-*block*-*tert*-butoxystyrene) (PS-*b*-PtBS) having different molecular weights and

TABLE 1 The Molecular Weights and the Compositions of PS-*b*-PtBS and PS-*b*-PtBS-*b*-PS

Sample	Target M_n of PS- <i>b</i> -PtBS (Target M_n of PS- <i>b</i> -sPHS ^a)	M_n (PDI) of PS ^b (GPC)	M_n of PtBS ^c (NMR)	Total M_n ^d	M_n (PDI) of BCP ^b (GPC)
P3-1	30k-10k (30k-14k)	28,400 (1.28)	9,200	37,600	36,800 (1.21)
P6-1	60k-13k (60k-19k)	47,900 (1.03)	10,900	58,800	56,700 (1.04)
P6-2	60k-20k (60k-28k)	54,900 (1.14)	17,000	71,900	75,300 (1.10)
P6-4	60k-40k (60k-56k)	52,100 (1.17)	40,800	92,900	99,600 (1.15)
P9-3	90k-30k (90k-42k)	85,100 (1.17)	28,400	113,500	118,500 (1.15)
P12-4	120k-40k (120k-56k)	128,000 (1.07)	44,900	172,900	146,800 (1.06)
P30-10	300k-100k (300k-139k)	319,300 (1.08)	103,000	422,300	364,600 (1.09)
P3-2-3 ^e	30k-20k-30k (30k-28k-30k)	26,500	16,800	69,800	64,800 (1.30)

^a Assuming the degree of sulfonation is 100%.

^b Determined from GPC.

^c Calculated from the integration areas in the ¹H NMR spectrum.

^d The summation of M_n of PS and M_n of PtBS calculated from NMR spectrum.

^e M_n of PtBS was measured from GPC and M_n of PS = [M_n of BCP (obtained from GPC) - M_n of PtBS]/2.

compositions. The following analogous reactions and sulfone chemistry were adopted to afford the product PS-*b*-sPHS. The corresponding PEMs were prepared from PS-*b*-sPHS with the sulfonic acids in either potassium salts (PS-*b*-sPHS-K) or tetra-ammonia salts (PS-*b*-sPHS-NR₄) via solvent casting and the following treatment to recover the acidity for all further measurements of membrane properties. The membranes prepared from PS-*b*-sPHS-K, denoted as K-membranes, generally exhibited less ordered morphologies while those made from PS-*b*-sPHS-NR₄ (N-membranes) showed more organized morphologies. Nevertheless, the presence of alkyl spacers resulted in complicated microphase separation behaviors, leading to some unique morphologies and enlarged domain sizes comparing to the corresponding sSEBS membranes. In comparison with the s-SEBS membrane having similar IEC, the N-membranes exhibited higher proton conductivity. In addition, all the membranes exhibited methanol permeability much smaller than that of Nafion 117 and s-SEBS. The enhancement in transport properties were suggested to be contributed by both the self-assembled morphologies and the flexibility of the alkyl spacers.

RESULTS AND DISCUSSION

Molecular Design, Synthesis and Characterization

The molecular weights, compositions and polydispersity index (PDI) of PS-*b*-PtBS are summarized in Table 1. PS-*b*-PtBS were named as PX-Y, where X indicates the target molecular weight of polystyrene segment while Y refers to the target molecular weight of PtBS segment. For example, P3-1 represents the PS-*b*-PtBS consisted of a PS block with the target molecular weight of 30 kg/mol and a PtBS block with the target molecular weight of 10 kg/mol. P3-1, P6-2, P9-3, P12-4, and P30-10, having the ratio of the target molecular weight of PS to PtBS fixed at 3/1, were designed to investigate the effect of molecular weight on the morphologies and the transport properties of the membranes. Based on the assumption that the degree of sulfonation is 100 mol % (each repeating unit in sPHS is modified with an alkylsulfonated group) and the densities of PS and sPHS are similar,

the volume fraction of the sPHS segment is ~31%. According to the phase diagram based on the mean-field theory regardless the interactions between sulfonic acids, these PS-*b*-sPHS were expected to exhibit morphologies with sPHS cylinders embedded in PS matrix, resulting in continuous ionic channels for proton transportation. P6-1, P6-2, and P6-4, having the same molecular weight of PS but different chain lengths of PtBS, were designed to exhibit different morphologies for evaluation of the interplays between the morphologies and the transport properties of the membranes. P3-2-3 was designed to possess composition similar to P6-2 to study the differences between triblock and diblock polyelectrolytes. To evaluate the effect of alkyl spacers of pendant alkylsulfonated groups, P6-2 and P9-3 were intentionally designed to match the molecular weights of the corresponding s-SEBS containing ~30 wt % of PS reported in the literature.^{18,19}

The molecular weight and the polydispersity of PS as well as the molecular weight distribution (PDI) of PS-*b*-PtBS were obtained from GPC. The molecular weight of PtBS was calculated from the ratio of the number of repeating units in PtBS to that in PS as suggested by ¹H NMR spectrum (see Supporting Information for detail calculations). All PS-*b*-PtBS possessed compositions close to the corresponding targets and narrow molecular weight distributions. The ¹H NMR spectrum of P6-4 and the consequent deprotected polymer PS-*b*-PHS are shown in Figure 1. The successful deprotection of *tert*-butyl group was confirmed by the absence of the characteristic signal of *tert*-butyl group at $\delta = 1.25$ ppm in Figure 1(b). After the attachment of alkylsulfonated groups to PHS backbone using sulfone chemistry and following post-treatments, the resulting PS-*b*-sPHS would have the sulfonic acids in various forms, including -SO₃H, -SO₃K and -SO₃NR₄. PS-*b*-sPHS were denoted as PX-Y-Z where Z (= H, K or NR₄) indicates the form of sulfonic acids. The degree of sulfonation (DS, the ratio of the number of repeating units attached with alkylsulfonated group in PHS to the total number of repeating units in PHS) was calculated using eq 1:

$$\text{DS\%} = \frac{\text{sulfur (wt \%)/carbon (wt \%)} \text{ obtained from element analysis}}{\text{theoretical value of sulfur (wt \%)/carbon (wt \%)} \text{ based on 100\% DS}} \times 100\% \quad (1)$$

The theoretical weight ratio of sulfur to carbon based on 100% DS could be obtained using the following estimation. The molar ratio of PS to sPHS, that is, the ratio of the number of repeating units in polystyrene to that in sPHS, was identical to the molar ratio of PS to PtBS calculated from the ^1H NMR spectrum of PS-*b*-PtBS based on the assumption that every repeating unit in PtBS was successfully deprotected and modified with an alkylsulfonated group. The molar number of sulfur in PS-*b*-sPHS was equivalent to the molar number of repeating units of sPHS since only sPHS contained sulfur. The molar number of carbon was the sum of the number of carbon (8) in a repeating unit in PS times the number of repeating units in PS and that in a repeating unit (11) in sPHS times the number of repeating units in sPHS. Hence, the molar ratio of sulfur to carbon should equal to $1/[11 + (\text{the molar ratio of PS to sPHS}) \times 8]$. The theoretical weight ratio of sulfur to carbon could be calculated from eq 2:

Weight ratio of S to C

$$\begin{aligned} &= \frac{\text{molar number of sulfur} \times \text{molar weight of sulfur}}{\text{molar number of carbon} \times \text{molar weight of carbon}} \\ &= \text{molar ratio of } \frac{\text{S}}{\text{C}} \times \frac{32}{12} \quad (2) \end{aligned}$$

Table 2 lists the theoretical and the experimental weight ratio of S to C, as well as the calculated degree of sulfonation. The DS of all PS-*b*-sPHS were close or above 100%, suggest-

ing the attachment of alkylsulfonated group using sulfone chemistry with mild reaction conditions was highly effective.

Preparation of Membranes

PS-*b*-sPHS with sulfonic acids in $-\text{SO}_3\text{H}$ form were insoluble in most common organic solvents and solvent combinations owing to the very distinctive solubility between the two building segments. Hence, the sulfonic acids needed to convert to the corresponding $-\text{SO}_3\text{K}$ or $-\text{SO}_3\text{NR}_4$ salts to promote the solubility of sPHS segment in organic solvents. P6-1-K could not afford the corresponding membrane because of the difficulty in dispersing P6-1-K in solvents. The membrane made from P6-4-K was too brittle to perform further measurements owing to the high content of sPHS. The successful conversion of $-\text{SO}_3\text{H}$ to $-\text{SO}_3\text{NR}_4$ could be suggested by the presence of characteristic peaks corresponding to the alkyl groups of tetrapropylammonium salts in the ^1H NMR spectrum of PS-*b*-sPHS- NR_4 (R = propyl). Figure 2 illustrates the ^1H NMR spectrum of P6-4- NR_4 , where the three broad peaks at $\delta = 0.99$, 1.7, and 3.2 ppm corresponding to the propyl groups in $-\text{SO}_3\text{NR}_4$ are clearly observed. The molar ratio of nitrogen to sulfur (N/S), calculated from the elemental analysis results listed in Table 3, could describe the degree of complex of NR_4^+ to SO_3^- (i.e., the number of NR_4^+ attached to a SO_3^-). The N/S ratios of all PS-*b*-sPHS- NR_4 were less than unity, indicating not every SO_3^- would bond with one NR_4^+ due to the bulkiness of NR_4^+ . In general, the degree of complex was around 50–70% except P6-1- NR_4

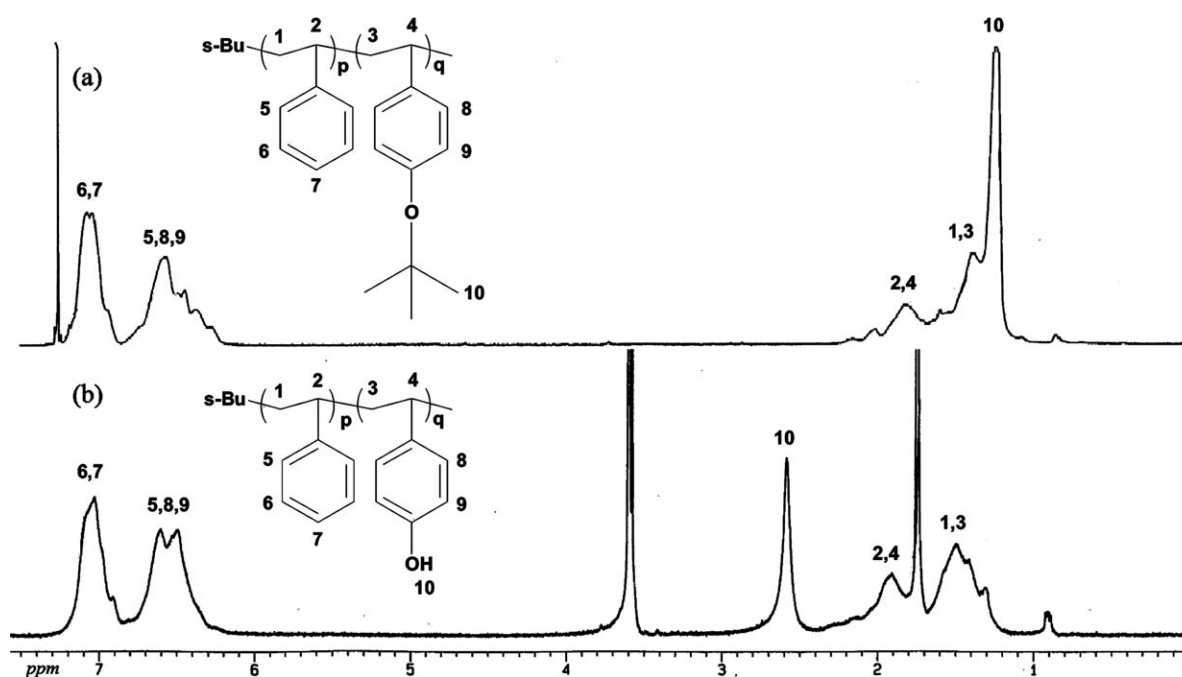


FIGURE 1 ^1H NMR spectrum of (a) P6-4; and (b) the corresponding PS-*b*-PHS.

TABLE 2 Elemental Analysis Results and the Degree of Sulfonation of PS-*b*-sPHS-K

Sample	Theoretical Calculation			Elemental Analysis			DS (%) ^a	M_n of PS- <i>b</i> -sPHS-K ^b
	Molar Ratio of PS/sPHS	Molar Ratio of S/C	Weight Ratio of S/C $\times 10^2$	C (wt %)	S (wt %)	Weight Ratio of S/C $\times 10^2$		
P3-1-K	5.23	1/52.84	5.05	73.11	3.67	5.02	99	28,400–14,600
P6-1-K	7.47	1/70.76	3.77	59.84	2.35	3.93	104	47,900–17,300
P6-2-K	5.48	1/54.84	4.86	72.92	3.51	4.81	99	54,900–26,700
P6-4-K	2.16	1/28.28	9.43	62.24	5.49	8.82	94	52,100–65,000
P9-3-K	5.08	1/51.64	5.16	72.79	3.50	4.81	93	85,100–44,700
P12-4-K	4.82	1/49.56	5.38	67.49	4.11	6.09	113	128,000–71,500
P30-10-K	5.25	1/53.00	5.03	68.08	5.97	8.77	174	319,300–164,100
P3-2-3-K	5.33	1/53.64	4.97	72.40	3.44	4.75	96	53,000–26,300

^a Calculated from the division of the weight ratio of S/C from elemental analysis by the theoretical weight ratio of S/C.

^b Based on the experimental DS%

with the lowest content of sPHS, showing the degree of complex $\sim 30\%$. Nevertheless, the partial chelating between NR_4^+ and SO_3^- enabled the resulting samples soluble in many organic solvents except P30-10-NR₄ having the largest molecular weight. The membranes were named as NX-Y (N-membranes) and KX-Y (K-membranes), representing those prepared from PS-*b*-sPHS-NR₄ and PS-*b*-sPHS-K, respectively. Before the measurements of transport properties and the morphology studies, all $-\text{SO}_3\text{K}$ and $-\text{SO}_3\text{NR}_4$ were converted to SO_3H by thorough acid wash.

Morphologies of Membranes

Figures 3 and 4 show the TEM images of dry N-membranes and K-membranes with sulfonic acids in $-\text{SO}_3\text{H}$ form. The microtomed thin slices were treated with lead acetate to stain the sulfonic acid rich domains, which appeared dark in the TEM images. The speckles observed might attribute to

the presence of lead carbonate³⁸ as the lead ion would inevitably react with CO_2 in air during the staining process. In general, the N-membranes exhibited more well-defined morphologies while the K-membranes possessed less-ordered morphologies, as a consequence of better solubility of sPHS-NR₄ in organic solvent comparing to sPHS-K.

N3-1 [Fig. 3(a)] exhibited a lamellae-like morphology with alternative dark and bright strips aligned in parallel. The dark strips, around 40 nm wide, were composed of spheres connected in a serial fashion, resembling strings of beads. The formation of the spheres might result from the strong interaction between sulfonic acids in sPHS-NR₄ segment owing to the smaller degree of complex of NR_4^+ to SO_3^- . Both N6-2 [Fig. 3(c)] and N9-3 [Fig. 3(e)] showed well-organized lamellae morphologies with the periodicity ~ 250 nm for the former and ~ 300 nm for the latter. N12-4,

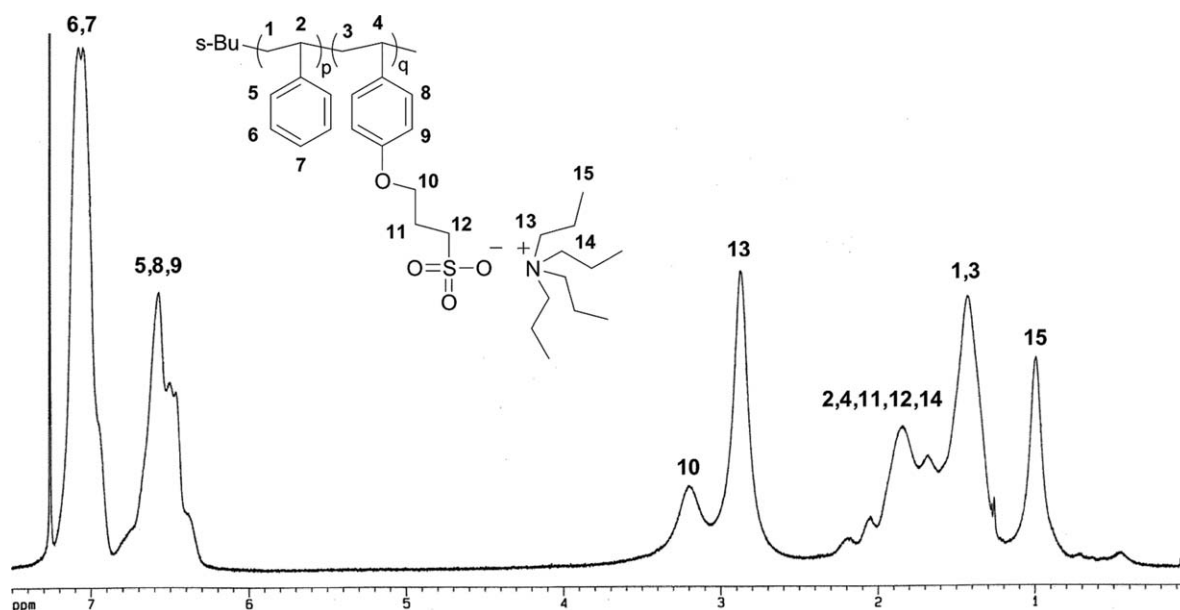
**FIGURE 2** ¹H NMR spectrum of P12-4-NR₄ in CDCl_3 .

TABLE 3 Elemental Analysis Results and Degree of Complex (DC) of NR₄⁺ to SO₃⁻ in PS-*b*-sPHS-NR₄

Sample	Elemental Analysis		Degree of Complex (DC = Molar Ratio of N/S) ^a	Calculations Based on DC	
	S (wt %)	N (wt %)		M _n of PS- <i>b</i> -sPHS-NR ₄	Weight % of sPHS-NR ₄
P3-1-NR ₄	3.50	0.54	0.357	28,400–17,400	38.0
P6-1-NR ₄	2.86	0.45	0.323	47,900–20,200	29.7
P6-2-NR ₄	3.70	0.87	0.526	54,900–34,500	38.6
P6-4-NR ₄	4.11	1.03	0.556	52,100–83,900	61.7
P9-3-NR ₄	3.89	1.06	0.625	85,100–60,000	41.4
P12-4-NR ₄	3.18	1.17	0.833	128,000–102,800	44.6
P30-10-NR ₄	3.18	0.99	0.714	319,300–225,600	41.4

^a DC described the number of NR₄⁺ attached to a SO₃⁻, which could be obtained from the molar ratio of N/S suggested by elemental analysis results as [N (wt %)/14]/[S (wt %)/32].

interestingly, showed a less-organized microstructure having parallel dark and bright strips arranged alternatively despite the expectation for a ordered lamellae morphology. The dark strips, averaging 200–300 nm in width, were composed of interconnected short-worms, and each worm contained several to tens of beads (spheres). The formation of beads might associate with the large molecular weight leading to more interaction between sulfonic acids in sPHS-NR₄ to produce aggregations of sulfonic acids despite a good degree of complex of NR₄⁺ to SO₃⁻. All the above four N-membranes prepared from PS-*b*-sPHS-NR₄ having similar compositions but different molecular weights showed different morphologies, suggesting factors affecting the resulting microstructures are more complicated than the incompatibility between the two constituting blocks. For N6-1, N6-2, and N6-4, prepared from PS-*b*-sPHS-NR₄ having similar PS block and dif-

ferent lengths of sPHS segments, the microstructures were found to be determined by the molecular weight ratio between PS and sPHS. N6-1 showed an ill-defined morphology with discontinuous sPHS domains dispersed in PS matrices, although sPHS cylindrical morphology was expected according to ~30 wt % content of sPHS-NR₄ in P6-1-NR₄. The high degree of sulfonation, the pendant flexible spacers and the low degree of complex of NR₄⁺ to SO₃⁻ would all contribute to a much stronger interaction between sulfonic acids to disrupt the regularity of the morphology. In Figure 3(d), N6-4 exhibited a cylindrical morphology with PS embedded in sPHS matrix despite the expectation for a lamellae morphology based on 62 wt % of sPHS-NR₄ in P6-4-NR₄. The high volume fraction of sPHS-NR₄ might attribute to the bulkiness of NR₄ to occupy more volume and to prevent coiling of sPHS-NR₄.

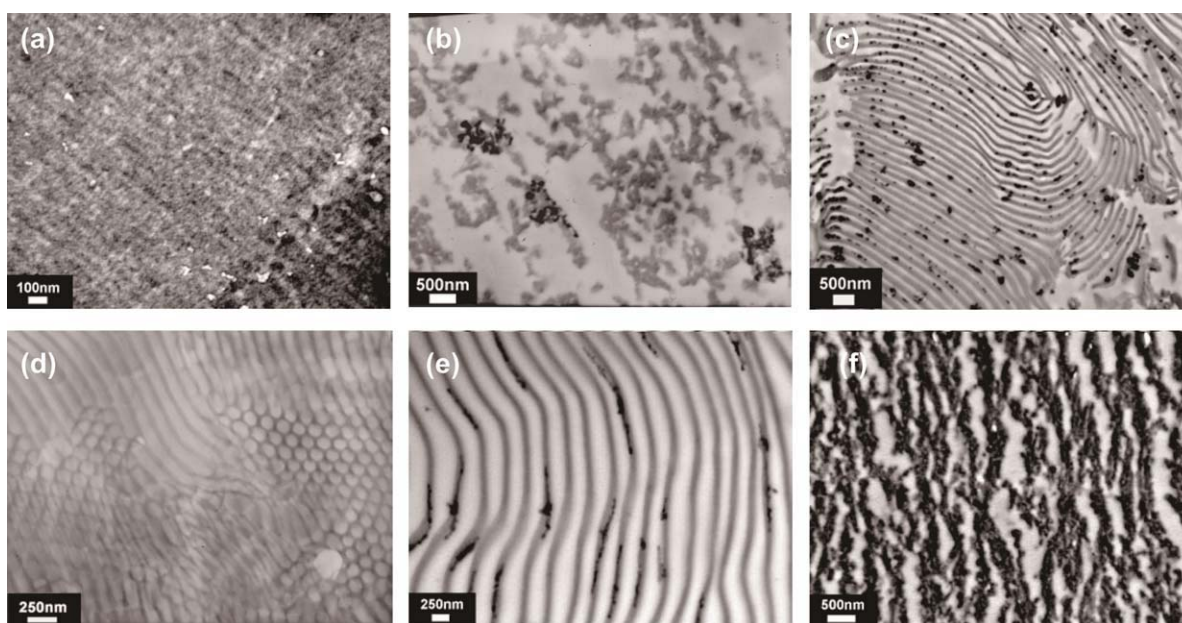


FIGURE 3 Cross-sectional TEM images of N-membranes: (a) N3-1, (b) N6-1, (c) N6-2, (d) N6-4, (e) N9-3, (f) N12-4. The dark areas represent the sPHS-rich domains.

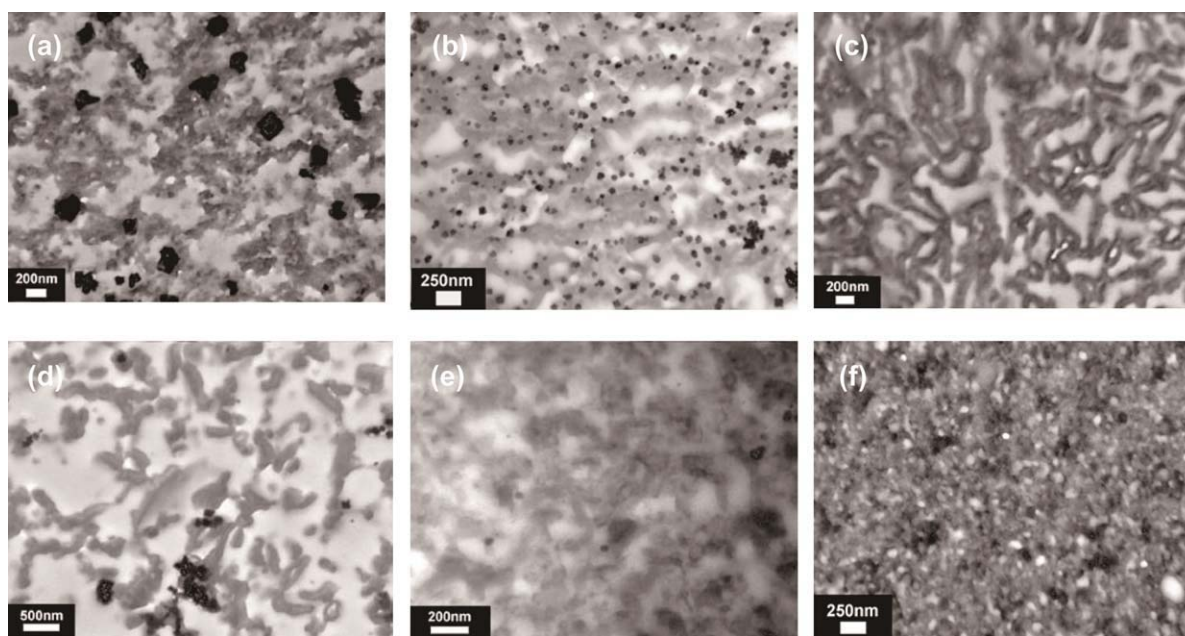


FIGURE 4 Cross-sectional TEM images of K-membranes: (a) K3-1, (b) K6-2, (c) K9-3, (d) K12-4, (e) K30-10, (f) K3-2-3. The dark regions represent the sPHS-rich domains.

In contrast to the N-membranes, K-membranes generally showed morphologies having sPHS domains dispersing in PS matrix with poor arrangements and some continuity. The sizes of the sPHS domains, around 100–300 nm, did not have clear correlations with the molecular weights. The lack of organization in the morphologies could be attributed to the self-aggregation of sPHS-K, much stronger than the microphase segregation of the block copolymer, dominating the driving forces for the microstructure formation. Interestingly, the sPHS domains in K9-3 [Fig. 4(c)] and K12-4 [Fig. 4(d)] formed hallow channels, which might result from the stronger microphase separation between PS and sPHS-K due to the larger molecular weights to compete with the self-aggregation of sPHS-K. In K3-2-3, prepared from the triblock copolymer P3-2-3-K having compositions and molecular weights similar to P6-2-K, the sPHS domains (dark areas) were randomly distributed in the PS matrix [Fig. 4(f)] with much smaller domain sizes in comparison with K6-2 [Fig. 4(b)], suggesting a denser packed microstructure owing to the physical crosslinking of a ABA triblock copolymer.³⁹

Small angle X-ray scattering (SAXS) studies, whose patterns are shown in Figure 5, were performed on unstained dry N-membranes to further investigate the morphological information to exclude the artificial effect cause by staining in the TEM studies. For N3-1, only a broad peak at q_1 corresponding to a d-spacing of 36 nm was observed, suggesting a less ordered microstructure in accordance with the morphology depicted by the TEM image showing lamellar-like arrangement of beads. N6-2 and N9-3 showed clear patterns with distinct peaks at $q_1, 2q_1, 3q_1, \dots$, where q_1 was referred to the Bragg spacing of 62 and 85 nm for N6-2 and N9-3, respectively. These scattering patterns typically suggested lamellar morphologies, in agreement with the observation from TEM.

Nevertheless, the d-spacings determined from the SAXS studies were much smaller than the periodicities of the lamellae observed from TEM. N12-4 exhibited a broad peak corresponding to a d-spacing of 80 nm, indicating a less ordered morphology. For N6-4, scattering peaks at $q_1, \sqrt{3}q_1$ were detected with $q_1 = 0.015$ referring to d-spacing = 42 nm, which suggested a cylindrical morphology. Although the morphologies suggested by SAXS studies and by TEM studies were generally in good agreement, the periodicities determined from the SAXS patterns were smaller than those identified by the TEM studies by two to three times. The remarkable differences in domain sizes have not been observed in the s-SEBS systems.^{21,40} Unfortunately, SAXS could not be performed on the stained samples to further verify the origin

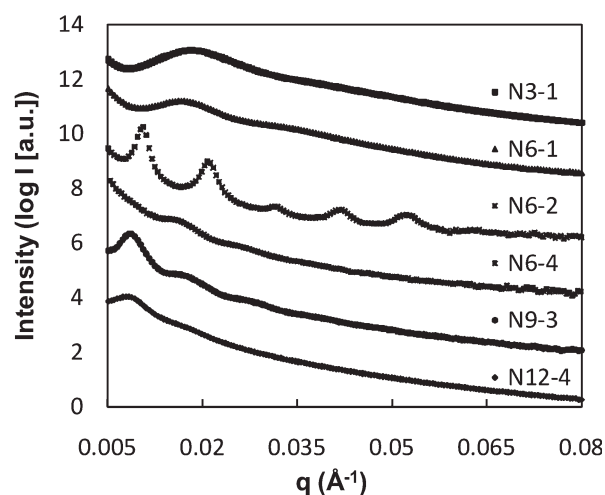


FIGURE 5 SAXS of dry N-membranes.

TABLE 4 Transport Properties of the Membranes Prepared from PS-*b*-sPHS

Membranes	IEC ^b (mmol/g)	WU (%)	MU (%)	λ_w	$\sigma \times 10^2$ (S/cm)	MP $\times 10^6$ (cm ² /s)	WP $\times 10^6$ (cm ² /s)	$\Phi \times 10^{-4}$ (S s/cm ³)
Nafion117	0.91	25	79	15.2	10.62	4.85	1.20	2.18
s-SEBS ^a	0.98	98	360	55.6	3.80	1.70	-	2.24
N3-1	1.05	69	127	36.5	4.64	1.29	1.72	3.60
N6-1	0.76	14	44	10.2	0.41	0.10	0.02	4.10
N6-2	1.09	60	80	29.3	3.64	0.98	1.97	3.71
N6-4	1.87	166	218	49.3	10.46	2.82	5.35	3.71
N9-3	1.01	58	72	31.9	4.37	0.83	2.32	5.27
N12-4	1.00	32	60	17.6	6.63	0.58	1.45	11.43
K3-1	1.09	56	75	28.6	6.24	0.58	1.33	10.76
K6-2	1.11	38	62	18.7	2.02	0.65	1.21	3.11
K9-3	1.01	71	86	39.1	3.13	0.56	1.01	5.59
K12-4	0.97	38	43	21.8	2.02	0.34	0.74	5.94
K30-10	1.04	51	60	27.2	1.54	0.57	1.54	2.70
K3-2-3	1.09	44	60	22.2	3.90	0.45	0.87	8.67

^a Retrieved from ref. 22.^b By titration.

of the discrepancy since the very strong contrast between stained sPHS domains and unstained PS domains leading to signal intensities exceeded the limit of the instrument. This difference might possibly result from the stretch of flexible spacers upon staining to direct the sulfonic acids away from the polymer backbone to reduce the packing density. Once the sulfonic acids bonded with lead ions, the stretched alkyl chains would retain extension after drying to result in larger domain sizes for the stained samples.

By comparing the domain sizes of the s-SEBS membranes and those of N-membranes having similar molecular weights and compositions, the formers were apparently smaller than the lateres. For example, the membrane casting from s-SEBS ($M_w \sim 118,000$, 28 wt % PS, 42 mol % DS) dispersing in a 80/20 THF/MeOH cosolvent exhibited a lamellar microstructure with the ionic domain in ~ 8 nm and the lamellar thickness in ~ 30 nm,^{21,22} while the periodicity of the lamellae in N9-3 was ~ 85 nm as suggested by the SAXS studies. The much larger domain size in N-membranes could be attributed to the presence of alkyl spacers as well as the bulkiness of NR₄ to occupy more spaces during the formation of membranes.

Transport Properties of the Membranes

Table 4 summarizes the transport properties of the N-membranes and K-membranes in protonated forms. The membranes prepared from P3-1-Z, P6-2-Z, P9-3-Z, P12-4-Z, and P30-10-Z (Z = NR₄ or K), possessing similar compositions but different molecular weights exhibited similar IEC (1.0–1.1 mmol/g) slightly smaller than the theoretical IEC (~ 1.2 mmol/g) based on 100% degree of sulfonation. The measured IEC values for N6-1 and N6-4 were 0.76 and 1.87, which were also slightly smaller than the theoretical values of 0.9 and 2.0, respectively. The proximity of the experimen-

tal and the theoretical IEC values also suggested the high degree of sulfonation.

Figure 6(a,b) show the water uptake (WU) and the methanol uptake (MU) of N- and K-membranes of P3-1-H, P6-2-H, P9-3-H, P12-4-H, and P30-10-H, respectively. WU (32–71%) of both N- and K-membranes were higher than WU of Nafion 117 (25%), indicating the greater water affinities in these membranes. As suggested by the TEM images and the SAXS studies, pendant alkylsulfonated side chains would expand the size of proton conducting channels resulting in an increase in the volumes for water absorption. Nevertheless, the WU of these membranes were smaller than that (98%) of the s-SEBS membrane having similar IEC, which might infer the pendant alkylsulfonated side chains would suppress the swelling of the membranes. For N-membranes, the increment in molecular weight of the block polyelectrolyte would lead to the suppression in WU due to the dimensional stabilization by the larger hydrophobic domains. For K-membranes, no clear trend was observed for WU as a function of molecular weight. Considering the membranes prepared from the same PS-*b*-sPHS with the sulfonic acids in different forms, N3-1 and N6-2 exhibited higher WU than their counterparts in K-membranes; while K9-3 and K12-4 showed larger WU than the corresponding N-membranes. The above observation might attribute to the variance in morphologies: the ordered morphologies in N3-1 and N6-2 would assist the water absorption through well-connected hydrophilic domains; while the hallow channels in K9-3 and K12-4 might function as water reservoirs to further enhance the water uptake. Except N3-1, all the membranes exhibited MU lower than or close to that of Nafion 117 ($\sim 78\%$) and much smaller than that of s-SEBS ($\sim 300\%$). The trends for MU regarding the effect of molecular weights are similar to those for WU. In contrast to Nafion 117 and s-SEBS, whose MU is almost triple of the WU, MU of these PS-*b*-sPHS membranes are only slightly higher than WU, suggesting the

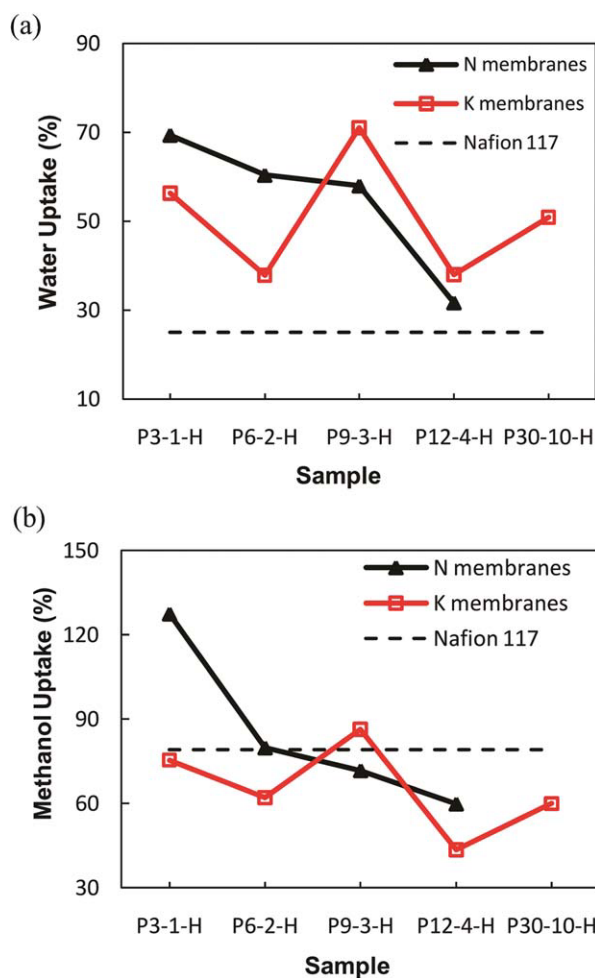


FIGURE 6 (a) Water uptake and (b) methanol uptake of membranes N3-1, N6-2, N9-3, N12-4 and K3-1, K6-2, K9-3, K12-4, K30-10. [Color figure can be viewed in the online issue, which is available at wileyonlinelibrary.com.]

pendant alkylsulfonated groups could result in relative high WU and low MU.

Figure 7 shows the proton conductivity (σ) measured at room temperature and 100% relative humidity as well as the methanol permeability (MP) of the N- and K-membranes of P3-1-H, P6-2-H, P9-3-H, P12-4-H, and P30-10-H. The N-membranes exhibited higher proton conductivities than their counterparts of K-membranes except N3-1, suggesting the well-organized morphologies in the formers should assist the proton conduction. The proton conductivities of those N-membranes were smaller than that of Nafion 117 but in the same order of magnitude owing to the weaker acidity of alkylsulfonic acids in comparison with fluorosulfonic acids. Nevertheless, these membranes exhibiting ordered morphologies possessed higher proton conductivities than the s-SEBS membranes, which could be attributed to both the larger domain sizes as well as the alkylsulfonated side chains promoting the relay motion of protons since the alkyl spacers could serve as pendulum to enhance the movement of sulfonic acids. Among these membranes, N12-4 exhibited the largest proton conduc-

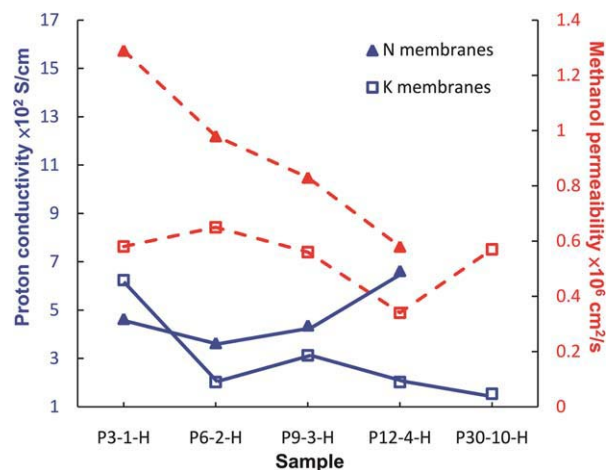


FIGURE 7 Proton conductivity and methanol permeability (MP) of membranes N3-1, N6-2, N9-3, N12-4 and K3-1, K6-2, K9-3, K12-4, K30-10. The solid lines represent the proton conductivity and the dashed lines represent the methanol permeability.

tivity despite the lowest WU. The proton conductivity is usually strongly dependent upon the amount of water absorbed in the membrane when vehicular mechanism predominantly contributes to the proton conduction. Hence, the above observation might infer that the relay mechanism participated more progressively in the proton conduction in N12-4 for more efficient utilization of sulfonic acids, which might owing to the unique morphology. For K-membranes showing less-ordered morphologies, the proportionality between the proton conductivity and the WU stood as expected.

The temperature dependent proton conductivities of N9-3 and N12-4 at relative humidity 60% ranging from 20 to 100 °C, shown in Figure 8, were higher than those of Nafion 117 through all the temperature range and which increased with

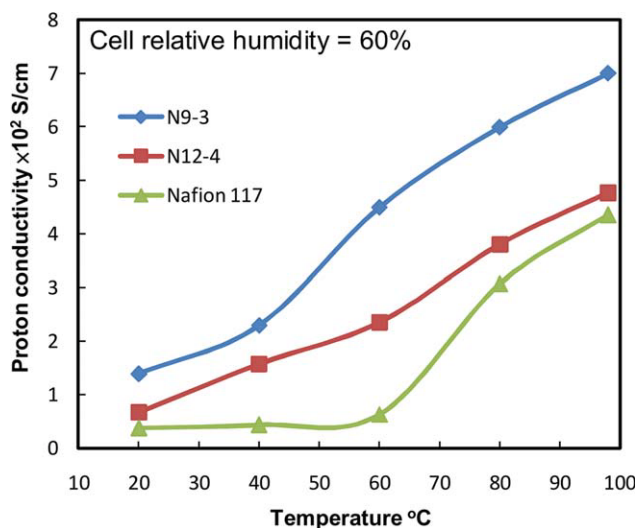


FIGURE 8 Temperature dependent proton conductivity of N9-3, N12-4, and Nafion 117 at 60% relative humidity. [Color figure can be viewed in the online issue, which is available at wileyonlinelibrary.com.]

increasing temperature. It is worthy to point out that the pendant alkylsulfonated side chains distributed in the well-organized sPHS domains should assist the proton conduction at low relative humidity possibly through the movement of side chains and the formation of nano-water reservoirs within the sPHS domains, enabling these membranes good candidates for high temperature PEMFC. More investigations will be carried out to understand the origin of the enhancement in proton conductivity.

The methanol permeability of all the membranes, much smaller than that of Nafion 117, was found to closely relate to the propensity of MU. N-membranes exhibited higher MP than the corresponding K-membranes despite that K9-3 possessed a larger MU than N9-3. Since methanol molecules would permeate through the membrane via the hydrophilic channels preferentially, the well-organized morphologies in N-membranes could lead to more effective methanol transportation. These N membranes also showed MP only 1/2–1/3 of the MP of the s-SEBS membrane exhibiting well-organized morphology,²² suggesting the alkyl spacers in the pendant alkylsulfonic acids might assist the blockage of methanol transportation. One of the most interesting features of these new membranes is that the water permeability is larger than the methanol permeability by two to three times while the WP is only a quarter of the MP in Nafion 117, indicating these membranes possess higher water affinity to enhance back diffusion of water which could be helpful in water management for passive modules.

WU, MU and MP, and solvent permeability of N6-1, N6-2, and N6-4 were depicted in Figure 9(a), while IEC and proton conductivity of the above membranes were shown in Figure 9(b). As discussed above, IEC increased with the increment of the length of sPHS segment, leading to augmentation in all the mentioned properties. Although IEC of N6-2 (1.09) was only 1.4 times of IEC of N6-1 (0.76), the proton conductivity and MP for the former are almost 10 times higher than those for the later. In contrast, IEC of N6-4 (1.87) was 1.8 times higher than IEC of N6-2; however, the transport properties for N6-4 were only triple of the corresponding properties for N6-2. These changes in the transportation properties suggest the continuity of the proton conducting domains should play a significant role as N6-1 showed isolated sPHS domains while N6-2 showed well-organized lamellar morphology. It was noticed that, different from all the other membranes, the water permeability was only 1/5 of the methanol permeability of N6-1 due to the much smaller water uptake, indicating the continuity of the hydrophilic domains is more critical to the water transportation than to the methanol diffusion.

P3-2-3-H and P6-2-H possessed similar compositions and molecular weights except the former was a triblock copolymer while the later was a diblock one. Their corresponding membranes K3-2-3 and K6-2 showed similar IEC, WU, and MU; nevertheless, the former exhibited a higher proton conductivity and a lower methanol permeability. As suggested by the TEM studies, PS in K3-2-3 might form physical cross-

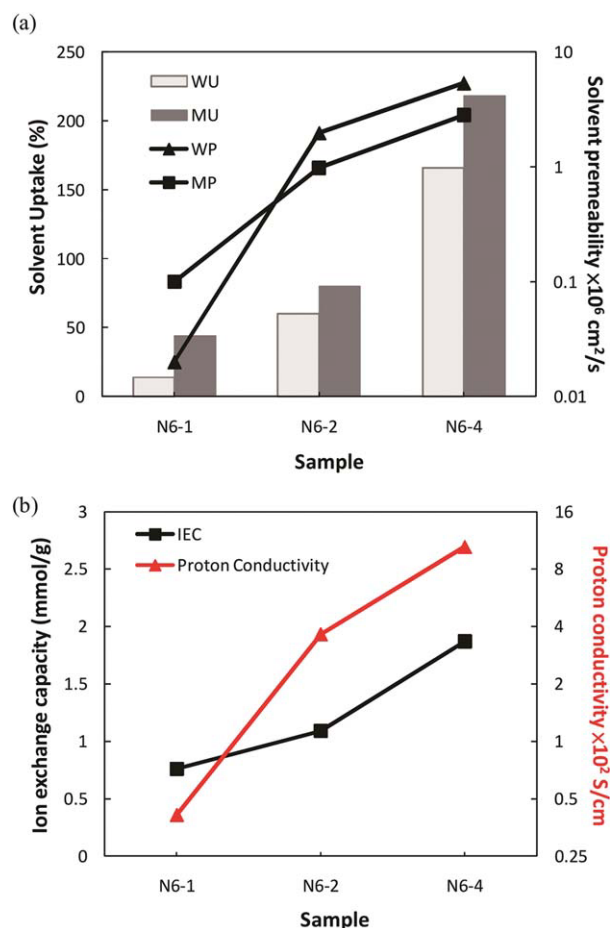


FIGURE 9 (a) Solvent uptake and solvent permeability; (b) IEC and proton conductivity of membranes N6-1, N6-2, and N6-4. [Color figure can be viewed in the online issue, which is available at wileyonlinelibrary.com.]

links to confine the domain sizes so that the methanol and water permeation were suppressed. Despite of the smaller hydrophilic domains, the higher proton conductivity of K3-2-3 might be contributed from the more pronounced relay motion of protons between the alkylsulfonated side chains.

The selectivity, interpreted as the ratio of the proton conductivity to the methanol permeability, has been generally considered as an efficiency indicator for a PEM. A membrane with a higher selectivity should have a higher potential for better fuel cell performance. As shown in Figure 10, the selectivity of all the membranes were better than that of Nafion 117. For N3-1, N6-2, N9-3, and N12-4, the larger molecular weight would lead to a higher selectivity since the increasing size of the hydrophobic domains would enhance the dimensional stability and thus suppress the methanol crossover. N12-4, despite a less-organized morphology, exhibited a much higher selectivity, which might attribute to its unique microstructure with interconnected hydrophilic beads where the linkages between beads might serve as bottlenecks for methanol transportation. For K3-1, K6-2, and K30-10 having similar irregular morphologies should have exhibited similar selectivity; nevertheless, K3-1 showed a much

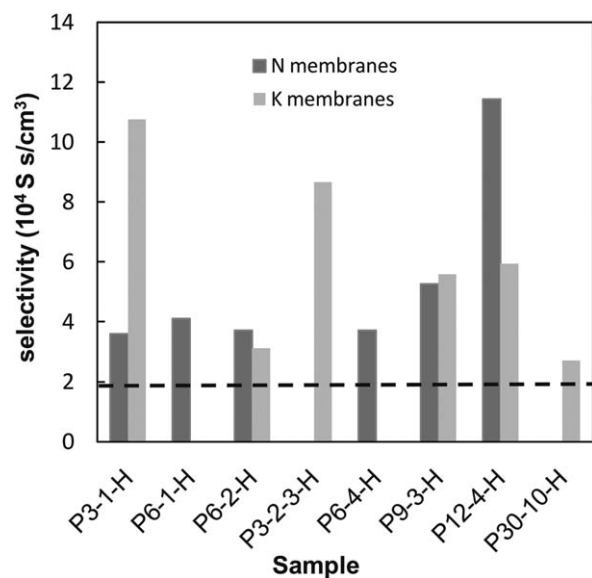


FIGURE 10 Selectivity of all membranes prepared. The dash line represents the selectivity of Nafion 117.

higher selectivity because of the high proton conductivity resulted from the unevenness of the membrane with sulfonic acids concentrated in the middle of the membrane. In contrast, the selectivity of K9-3 and K12-4 were twice higher than those of K6-2 and K30-10 because of the hollow channels for efficient proton transportation. For K3-2-3 and K6-2, the former made from the triblock copolymer showed selectivity almost triple of the later owing to the much densely packed morphology. It was noticed that the selectivities of N-membranes were not necessarily higher than the selectivities of their counterparts in K-membranes, suggesting that the membranes with well-organized morphologies might not be the best for the selectivity.

EXPERIMENTAL

Materials

All reagents were purchased from Aldrich, TCI, Alfa or Acros and used as received without further purification unless described specifically. All solvents were from ECHO or Mallinckrodt. Styrene (SHOWA, 99%+) and 4-*tert*-butoxystyrene (*t*BS) (Aldrich, 99%+) were purified by stirring with di-*n*-butylmagnesium for 24 h at room temperature under nitrogen. The dried monomers were distilled and stored in custom designed Rotaflor® reservoirs. Tetrahydrofuran (THF) was predried over calcium hydride and distilled from a mixture of sodium and benzophenone under nitrogen atmosphere.

Synthesis of PS-*b*-sPHS

The precursor poly(styrene-*block*-4-*tert*-butoxystyrene), denoted as PS-*b*-PtBS, was synthesized via anionic polymerization with sequential monomer addition at -78 °C in THF using *sec*-BuLi (1.3 M solution in cyclohexane) as the initiator. A general procedure is described below using P3-1, consisted of a polystyrene

segment with the target M_n of 30000 and a poly(4-*tert*-butoxystyrene) with the target M_n of 10,000, as an example.

Dried THF (200 mL) was distilled from the THF solution of living polystyryl anion and collected in a custom designed flask equipped with Rotoflo® stopcock. A suitable quantity of *sec*-BuLi was added at -78 °C to remove the impurities and the THF was then allowed to warm to room temperature slowly. *sec*-BuLi (232 μ L, 0.30 mmol) was added to the above THF at -78 °C under nitrogen and purified styrene (9.0 g, 87 mmol) was then transferred from the reservoir to the mixture at the same temperature. The polymerization of styrene was allowed to perform for 1 h and 1 mL polymer solution was transferred to 3 mL methanol for sampling. 4-*tert*-butoxystyrene (*t*BS, 3.0 g, 17 mmol) was transferred into the above polystyryl anion solution at -78 °C under nitrogen to undergo the polymerization of *t*BS. After another 1 h, anhydrous degassed methanol (2 mL) was added to terminate the polymerization. The crude block polymer was isolated by precipitation in methanol and the following filtration. Further purification through repeating dissolution-precipitation afforded the final product.

The *tert*-butyl group was removed by treating PS-*b*-PtBS (**1**) (12 g; 17.04 mmol of PtBS) with hydrochloric acid (37 wt % in water, 7.055 mL) in 200 mL 1,4-dioxane at 60 °C for 36 h. The crude product was obtained by precipitating the reaction mixture in hexane. The precipitates was then washed with copious amounts of water and dried under vacuum at 40 °C for 24 h to afford purified PS-*b*-PHS (**2**) (10.8 g). Yield: 95%.

The sulfonic acid groups were grafted onto the PHS segment by reacting PS-*b*-PHS (10.8 g; 17 mmol) with potassium hydride (3.6 g; 25 mmol) and 1,3-propanesultone (5.35 g; 34 mmol) in 150 mL anhydrous THF at 60 °C under nitrogen for 24 h. The excess KH was quenched by slow addition of hydrated methanol (20 mL). The reaction mixture was then pouring into a large amount of water to produce the precipitates as the crude product. The precipitates were collected and washed with hexane and methanol and dried under vacuum at 40 °C to afford purified PS-*b*-sPHS-K (**3**) (13.2 g). Yield: 94%.

Synthesis of sPHS-*b*-PS-*b*-sPHS

The synthesis of the triblock copolymer poly(4-*tert*-butoxystyrene-*block*-styrene-*block*-4-*tert*-butoxystyrene), PtBS-*b*-PS-*b*-PtBS, was similar to that of the diblock copolymer PS-*b*-PtBS except the mixture of sodium (1.25 g; 54 mmol)/naphthalene (6.4 g; 50 mmol) in 50 mL anhydrous THF was used instead of *sec*-BuLi as a bifunctional initiator. A small amount of the initiator solution was transferred to 15 mL methanol/water ($v/v = 1/2$) mixture and the above sampling mixture was titrated using 0.1 M diluted hydrochloric acid to identify the effectively concentration of the initiator as 0.85 M.⁴¹

Characterization of the Block Polyelectrolytes and the Precursors

Gel permeation chromatography (GPC) measurements were carried out using VISCOTEK HT-GPC module 350 with THF

as eluting solvent at 35 °C with an elution rate of 1 mL/min. Polystyrene standards were obtained from VISCOTEK for calibration. ¹H NMR spectra were obtained from BRUKER NRX-400 MHz spectrometer using CDCl₃ or THF-d₈ as solvent. Elemental analysis (EA) was performed with an HERAEUS VarioEL-III (N, C, S, and H elements) using Sulfanilic Acid and Acetanilide as standards.

Membrane Preparation

The membranes were prepared from solvent casting of PS-*b*-SPHS with sulfonic acids in the forms of potassium salts (denoted as PS-*b*-SPHS-K) and tetra-alkylammonium salts (denoted as PS-*b*-SPHS-NR₄). PS-*b*-SPHS-K was dispersed in *N*-methyl-2-pyrrolidone (NMP) at a concentration of 5 wt % and the corresponding membrane was obtained by heating the suspension at 50 °C for 2 h and then at 70 °C for 24 h. The membrane was further dried under vacuum at 60 °C for 48 h. PS-*b*-SPHS-NR₄ (**4**) was obtained by replacing K⁺ in SO₃K with NR₄⁺ according to the following procedure. Tetrapropylammonium hydroxide was added dropwise to a dispersion of PS-*b*-SPHS-K in CH₂Cl₂ until the dispersion became clear. The resulting mixture was stirred overnight at room temperature and then was concentrated to a small volume followed by the addition of methanol to afford the precipitates of PS-*b*-SPHS-NR₄. The membranes were obtained by heating a 5 wt % PS-*b*-SPHS-NR₄ solution in THF/NMP (w/w = 1/1) at 50 °C for 2 h, 60 °C for 12 h, and then 70 °C for 24 h. The membranes were then annealed at 120 °C under vacuum for 48 h. The sulfonic acids were regenerated by immersing the membranes in a 1.5 M H₂SO₄ solution at 50 °C for 24 h to exchange K⁺ and NR₄⁺ back into H⁺, and the membranes with sulfonated groups in acid form were then washed with DI water several times to remove the excess sulfuric acid.

Ion Exchange Capacity (IEC), Water and Methanol Sorption

A membrane was equilibrated in a saturated NaCl solution for 24 h at 40 °C to exchange protons with sodium ions. The resulting solution was titrated with 0.01 M NaOH using phenolphthalein as indicator. After titration, the membrane was placed in a 1.5 M H₂SO₄ solution for 24 h to reprotonate the membranes, and was then dried under vacuum for 12 h at 60 °C to measure the weight of the dry membrane. IEC of the membrane (mmol/g) was calculated according to eq 3.

$$\text{IEC} = \frac{M_{\text{NaOH}} V_{\text{NaOH}}}{W_{\text{dry}}} \quad (3)$$

where M_{NaOH} and V_{NaOH} are the molar concentration of NaOH solution and the volume used in titration, respectively. W_{dry} is the weight of the dry membrane with sulfonic acid in H form.¹⁷

The dry membrane was equilibrated in deionized water or 50 vol % methanol solution at 40 °C for 12 h and blotted with a Kimwipe to remove surface water to measure the weight of wet membrane. The water and the methanol

uptake of the membrane were calculated according to eqs 4 and 5, respectively.

$$\text{WU} (\%) = \frac{W_{\text{w}} - W_{\text{dry}}}{W_{\text{dry}}} \times 100\% \quad (4)$$

$$\text{MU} (\%) = \frac{W_{\text{M}} - W_{\text{dry}}}{W_{\text{dry}}} \times 100\% \quad (5)$$

The number of water molecules absorbed per ion exchange site (λ_{w}) was calculated using eq 6.

$$\lambda_{\text{w}} = \frac{\text{WU}}{\text{M}(18) \times \text{IEC}} \times 1000 \quad (6)$$

Electrochemical Impedance Spectroscopy⁴²

The proton conductivity of a membrane was measured at room temperature using Alternating-current (AC) impedance analyzer ZAHNER IM6eX with a through-plane setup attached the platinum electrode with 1 mm diameter. The impedance measurement was carried out from 3 MHz to 1 Hz at voltage amplitude of 10 mV. The membranes were immersed in deionized water at least 12 h before measurement. The conductivity was calculated from the ohmic resistance determined from the intercept of the real-imaginary impedance curve with impedance axis. The proton conductivity was obtained using the following eq 7.

$$\sigma = \frac{L}{R \times A} \quad (7)$$

where σ is the proton conductivity (S/cm), L is the thickness of membranes (cm), R is the ohmic resistance of the membrane (Ω) and A is the area of the electrode (cm²).

Temperature-varied data were collected using custom designed cell with a through-plane setup having two stainless electrodes (top electrode area = 0.0314 cm² and bottom electrode area = 0.785 cm²) in a environmental control oven. The sample was placed between the two separate electrodes in contact with only the bottom electrode, 1 h after the desired temperature and R.H. were reached, the top electrode was then pushed down to contact the sample. The EIS measurement was carried out after another 30 minutes to ensure the equilibrium condition. The dimensions of the samples were assumed to be constant through the experiments.

Methanol Permeability (MP) and Water Permeability (WP)

Methanol permeability was measured at room temperature by a side-by-side glass diffusion cell. Forty milliliter of 50 vol % methanol solution and 40 mL deionized water were placed at the two opposite sides of the membrane. Methanol flux and water flux were established across the membrane due to the concentration difference between the two compartments. After a certain period, usually 4–6 h, the weight of methanol diffuse from the methanol side to the water side and the weight of water diffuse from the water side to the methanol side can be obtained from the calculation

associated with the total weight and the concentration of methanol (wt %), measured by density/concentration meter (DMA N35 Anton paar), at each side before and after the experimental according to eqs 8 and 9, respectively.

$$W_{\text{MeOH,D}} = (\text{wt \%})_{\text{MeOH@W,F}} \times W_{\text{W,F}} \quad (8)$$

$$W_{\text{H}_2\text{O,D}} = W_{\text{W,I}} + W_{\text{W,F}} - W_{\text{MeOH,D}} \quad (9)$$

Where $W_{\text{W,I}}$ and $W_{\text{W,F}}$ are the weight of the solution at the water side before and after the experiment respectively; while $(\text{wt \%})_{\text{MeOH at W,F}}$ is the concentration (wt %) of MeOH in the solution at the water side after the experiment.

A model experiment was carried out within the experiment period for the crossover measurement to monitor the change of the methanol concentration versus time and a linear relationship was observed. Thus we could assume that the amount of water/methanol diffused through the membrane change linearly with time during the experiment. The methanol flux and the methanol permeability could be retrieved using eqs. 10 and 11, respectively.

$$\text{Flux}_{\text{MeOH}} = \frac{W_{\text{MeOH,D}}/M(32)}{A \times t} \quad (10)$$

$$P_{\text{MeOH}} = \frac{\text{Flux}_{\text{MeOH}} \times L}{\Delta C_{\text{MeOH}}} \quad (11)$$

where $W_{\text{MeOH,D}}$ is the total weight of methanol diffused, M is the molecular weight of methanol, t (sec) is the time allowed for the permeation experiment, A (cm^2) and L (cm) are the effective area for diffusion and the thickness of the membrane, ΔC_{MeOH} is the average difference in the molar concentration of methanol between the two sides of the membrane throughout the experimental period. The flux and the permeability of water can also be simultaneously obtained using the same equations by replacing $W_{\text{MeOH,D}}$ with $W_{\text{H}_2\text{O,D}}$, ΔC_{MeOH} with $\Delta C_{\text{H}_2\text{O}}$ and using $M(18)$ instead of $M(32)$.

The selectivity (Φ), evaluating the overall membrane performance, is defined by the following relationship:

$$\Phi (\text{S/cm}^3) = \frac{\sigma}{P} \quad (12)$$

where σ is the proton conductivity (S/cm) and P the methanol permeability (cm^2/s) through of the membrane.

Morphologies of Membranes, Transmission Electron Microscopy⁴³ and Small Angle X-Ray Scattering

A piece (1 mm \times 5 mm) of the membrane were stained by soaking it in a saturated lead acetate solution for 12 h with the following wash with DI water and drying under vacuum at 60 °C for 2 h.⁴⁴ TEM images of the microtomed thin slices were obtained from JOEL JEM-1230 TEM using an accelerating voltage of 100 kV with Gatan DualVision CCD Camera. Small angle X-ray scattering was performed at 23A1 beam line at the National Synchrotron Radiation Research Center (NSRRC) in Taiwan.⁴⁵ The X-ray beam of a vertical

divergence of 0.3 mrad was extracted from the superconducting wavelength shifter source and focused by an Rh-coated mirror to the detector position, with a focused beam size of 1.0 mm by 1.5 mm in the vertical and horizontal directions, respectively. Ge (111) double crystal monochromator was used for monochromating the beam for an energy about 39% for 7 keV photons was used to obtain photon numbers with a wave of $\lambda = 1.77 \text{ \AA}$ and an energy resolution $\Delta E/E$ of $\sim 10^{-3}$. The distance between the sample and the detector was 2.4 m. The wave vector transfer of scattered photons $q = 4\pi \sin(\theta/2)/\lambda$ is defined by the scattering angle θ and wavelength λ . Ag-behenate was used for the calibration of the q value.

CONCLUSIONS

A series of novel block polyelectrolyte PS-*b*-SPHS containing pendant alkylsulfonic acids with accurate molecular weight control, narrow polydispersity and high degree of sulfonation were successfully synthesized via anionic polymerization and the following analogous chemistry. In comparison with the accustomed postsulfonation, the sultone chemistry would lead to a highly-efficient sulfonation via a mild reaction. PEMs were prepared from PS-*b*-SPHS with sulfonic acids in potassium salts and tetraproylammonium salts; and the formers exhibited less ordered morphologies while the latter showed well-organized morphologies. The presence of the alkyl spacers and the columbic interactions between polyelectrolytes would complicate the microphase separation and hence resulted in some unique morphologies. The transport properties of the membranes were found to closely relate to the morphologies and the domain sizes, which were affected by various factors including the compositions, the molecular weights and the forms of the sulfonic acids. The more organized morphologies did lead to enhancement in proton conductivity and the continuity of the hydrophilic domains was found to critical to water permeation and effective proton transportation. Nevertheless, the organized morphologies did not necessarily provide the best selectivity. In addition, the movement of the pendent alkylsulfonic acid groups might also involve in the improvement of the transport properties. Comparing to the corresponding s-SEBS membrane having similar IEC, both N-membranes and K-membranes exhibited improved proton conductivities and methanol permeability in the order of $10^{-7} \text{ cm}^2/\text{s}$, leading to much improved selectivities. The best selectivity could be higher than that of Nafion 117 by five times at most.

This research was financially supported by the National Science Council of Taiwan (NSC 95-2623-7-002-018 and NSC 97-2623-7-002-015-ET). The authors thank Chih-Yuan Tang (Instrument Center, NTU) for the assistance with ultramicrotomy and R&D Center for Membrane Technology, CYCU for EIS measurement.

REFERENCES AND NOTES

- 1 Service, R. F. *Science* 2002, 296, 1222–1224.
- 2 Hickner, M. A.; Ghassemi, H.; Kim, Y. S.; Einsla, B. R.; McGrath, J. E. *Chem Rev* 2004, 104, 4587–4611.

- 3** Deluca, N. W.; Elabd, Y. A. *J Polym Sci Part B: Polym Phys* 2006, 44, 2201–2225.
- 4** Smitha, B.; Sridhar, S.; Khan, A. A. *J Memb Sci* 2005, 259, 10–26.
- 5** Larminie, J.; Dicks, A. *Fuel Cell Systems Explained*; Wiley: Chichester, 2003.
- 6** Ravikumar, M. K.; Shukla, A. K. *J Electrochem Soc* 1996, 143, 2601–2606.
- 7** Scott, K.; Taama, W.; Cruickshank, J. *J Appl Electrochem* 1998, 28, 289–297.
- 8** Ge, J. B.; Liu, H. T. *J Power Sources* 2005, 142, 56–69.
- 9** Kerres, J. A. *J Memb Sci* 2001, 185, 3–27.
- 10** Richard, B.; E. I. Du Pont de Nemours and Company, Wilmington, Del., US Patent 3,714,245, 1973.
- 11** Grot, W. G.; E. I. Du Pont de Nemours and Company, Wilmington, Del., US Patent 3,718,627, 1973.
- 12** Schuster, M. E.; Meyer, W. H. *Annu Rev Mater Res* 2003, 33, 233–261.
- 13** Leibler, L. *Macromolecules* 1980, 13, 1602–1617.
- 14** Darling, S. B. *Progr Polym Sci* 2007, 32, 1152–1204.
- 15** Hadjichristidis, N.; Pispas, S.; Floudas, G. *Block Copolymers: Synthetic Strategies, Physical Properties, and Applications*; Wiley-Interscience: Hoboken, NJ, 2003.
- 16** Kotz, J.; Kosmella, S.; Beitz, T. *Progr Polym Sci* 2001, 26, 1199–1232.
- 17** Abeysekera, R.; Bushby, R. J.; Caillet, C.; Hamley, I. W.; Lozman, O. R.; Lu, Z. B.; Robards, A. W. *Macromolecules* 2003, 36, 1526–1533.
- 18** Kim, J.; Kim, B.; Jung, B. *J Memb Sci* 2002, 207, 129–137.
- 19** Won, J.; Park, H. H.; Kim, Y. J.; Choi, S. W.; Ha, H. Y.; Oh, I. H.; Kim, H. S.; Kang, Y. S.; Ihn, K. J. *Macromolecules* 2003, 36, 3228–3234.
- 20** Kim, B.; Kim, J.; Cha, B. J.; Jung, B. *J Memb Sci* 2006, 280, 270–277.
- 21** Kim, J.; Kim, B.; Jung, B.; Kang, Y. S.; Ha, H. Y.; Oh, I. H.; Ihn, K. J. *Macromol Rapid Commun* 2002, 23, 753–756.
- 22** Harrison, W. L.; Hickner, M. A.; Kim, Y. S.; McGrath, J. E. *Fuel Cells* 2005, 5, 201–212.
- 23** Elabd, Y. A.; Napadensky, E.; Sloan, J. M.; Crawford, D. M.; Walker, C. W. *J Memb Sci* 2003, 217, 227–242.
- 24** Elabd, Y. A.; Walker, C. W.; Beyer, F. L. *J Memb Sci* 2004, 231, 181–188.
- 25** Wang, X. L.; Oh, I. K. *J Nanosci Nanotechnol* 2010, 10, 3203–3206.
- 26** Elabd, Y. A.; Napadensky, E.; Walker, C. W.; Winey, K. I. *Macromolecules* 2006, 39, 399–407.
- 27** Lee, W.; Kim, H.; Lee, H. *J Memb Sci* 2008, 320, 78–85.
- 28** Serpico, J. M.; Ehrenberg, S. G.; Fontanella, J. J.; Jiao, X.; Perahia, D.; McGrady, K. A.; Sanders, E. H.; Kellogg, G. E.; Wnek, G. E. *Macromolecules* 2002, 35, 5916–5921.
- 29** Nacher, A.; Escibano, P.; Del Rio, C.; Rodriguez, A.; Acosta, J. L. *J Polym Sci Part A: Polym Chem* 2003, 41, 2809–2815.
- 30** Rubatat, L.; Li, C. X.; Dietsch, H.; Nykanen, A.; Ruokolainen, J.; Mezzenga, R. *Macromolecules* 2008, 41, 8130–8137.
- 31** Park, M. J.; Downing, K. H.; Jackson, A.; Gomez, E. D.; Minor, A. M.; Cookson, D.; Weber, A. Z.; Balsara, N. P. *Nano Lett* 2007, 7, 3547–3552.
- 32** Park, M. J.; Nedoma, A. J.; Geissler, P. L.; Balsara, N. P.; Jackson, A.; Cookson, D. *Macromolecules* 2008, 41, 2271–2277.
- 33** Park, M. J.; Balsara, N. P. *Macromolecules* 2008, 41, 3678–3687.
- 34** Jouanneau, J.; Gonon, L.; Gebel, G.; Martin, V.; Mercier, R. *J Polym Sci Part A: Polym Chem* 2010, 48, 1732–1742.
- 35** Thomas, O. D.; Peckham, T. J.; Thanganathan, U.; Yang, Y. S.; Holdcroft, S. *J Polym Sci Part A: Polym Chem* 2010, 48, 3640–3650.
- 36** Lee, C. H.; Park, C. H.; Lee, Y. M. *J Memb Sci* 2008, 313, 199–206.
- 37** Dimitrov, I.; Jankova, K.; Hvilsted, S. *J Polym Sci Part A: Polym Chem* 2010, 48, 2044–2052.
- 38** Hayat, M. A. *Basic Techniques for Transmission Electron Microscopy*; Academic Press: Orlando, 1986.
- 39** Jannasch, P. *Polymer* 2002, 43, 6449–6453.
- 40** Kim, B.; Kim, J.; Jung, B. *J Memb Sci* 2005, 250, 175–182.
- 41** Lowrey, A. H.; George, C.; Dantonio, P.; Karle, J. *J Am Chem Soc* 1971, 93, 6399.
- 42** Yuan, X. Z.; Wang, H. J.; Sun, J. C.; Zhang, J. J. *Int J Hydrogen Energ* 2007, 32, 4365–4380.
- 43** Jutemar, E. P.; Jannasch, P. *J Memb Sci* 2010, 351, 87–95.
- 44** Lin, J.; Wu, P. H.; Wycisk, R.; Pintauro, P. N.; Shi, Z. Q. *Macromolecules* 2008, 41, 4284–4289.
- 45** Lai, Y. H.; Sun, Y. S.; Jeng, U.; Huang, Y. S.; Song, Y. F.; Dronyak, R.; Tsang, K. L.; Liang, K. S. *Nucl Instrum Method Phys Res Sect B: Beam Interact Mater Atoms* 2005, 238, 205–213.